Supplemental Information

Aerosol light absorption and the role of ELVOCs in the Eastern Mediterranean

Antonios Tasoglou[1,5], Evangelos Louvaris[2,3], Kalliopi Florou[2,3] Aikaterini Liangou[2,3], Eleni Karnezi[1] Christos Kaltsonoudis[4], Ningxin Wang[1], Spyros N. Pandis[1,2,3]

[1]Department of Chemical Engineering, Carnegie Mellon University, Pittsburgh
[2]Department of Chemical Engineering, University of Patras, Patras, Greece
[3] Institute of Chemical Engineering Sciences (ICE-HT), FORTH, Patras, Greece
[4]Department of Mechanical Engineering, Carnegie Mellon University, Pittsburgh, United States
[5]RJ Lee Group, Inc., Monroeville, United States

S1. Data analysis of TD measurements

The OA MFR is the ratio of OA concentration remaining after passing through the TD over the ambient OA concentration passing through the bypass line. The ambient OA concentrations were corrected for the AMS particle collection efficiency (CE_{amb}) calculated by the algorithm of Kostenidou et al. (2007). The average CE_{amb} value for the entire campaign was 0.64. The thermodenuded OA concentration was also corrected for the corresponding TD AMS collection efficiency (CE_{TD}) which was higher from the ambient and equal to 0.79 on average.

Figure S1 shows the collection efficiency-corrected ambient and TD OA mass concentrations. The TD temperature time series of the entire campaign is also shown. The ambient OA concentration was quite variable ranging from 0.25 to 2.5 μg m^{-3}. The average ambient OA concentration observed during this campaign (1.2 μg m^{-3}) was almost half of that during May 2008 in FAME-08 (Hildebrandt et al., 2010).

The MFR calculation assumes implicitly that the OA concentration remains constant during the measurement period. If two consecutive OA ambient mass concentrations differed by more than 25% the corresponding MFR was not included in the analysis. Also, in order to ensure that the temperature remained constant between two consecutive TD samples, the absolute difference between the two samples had to less than 5 °C. If this difference for a TD sample was higher, then the sample was not included in our analysis.

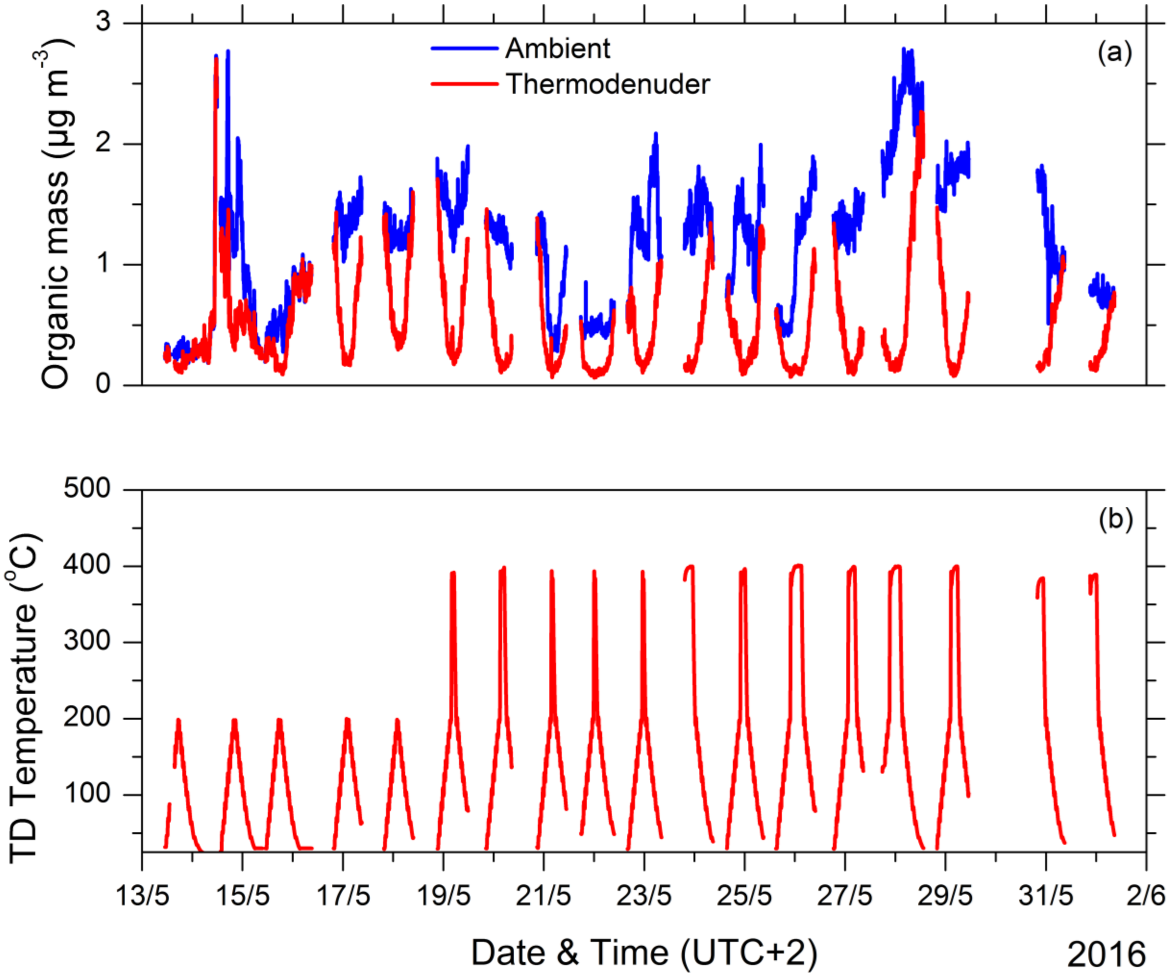

Figure S1: (a) Time series of the total ambient (blue line) and total thermodenuded (red line) OA mass concentration. (b) TD temperature during the measurement period.

The same quality control approach was used also for the factors resulting from the PMF analysis of the AMS spectra. However, in this case a minimum concentration threshold of 0.1 μg m^{-3} was used for the ambient concentrations together with the criterion of the stability of the ambient concentrations during the sampling period. MFR values corresponding to concentrations of the PMF factors below this threshold were eliminated from the analysis. These criteria still allowed us to use approximately 70% of the measured values. In the present work we analyzed the complete datasets together averaging the corresponding results.

The MFR values were corrected for particle losses in the TD. These number losses inside the TD are due to diffusion of the smaller particles to the walls, or deposition of the larger particles on the TD walls, and thermophoretic losses due to temperature differences (Burtscher et al., 2001). To account for these losses, sample flow rate as well as size- and temperature-dependent loss corrections were applied following Louvaris et al. (2017) corresponding to the operating conditions during the campaign. The final step of the data analysis was to average the corrected for CE and TD losses MFR data based on temperature bins of 10^{o}C.

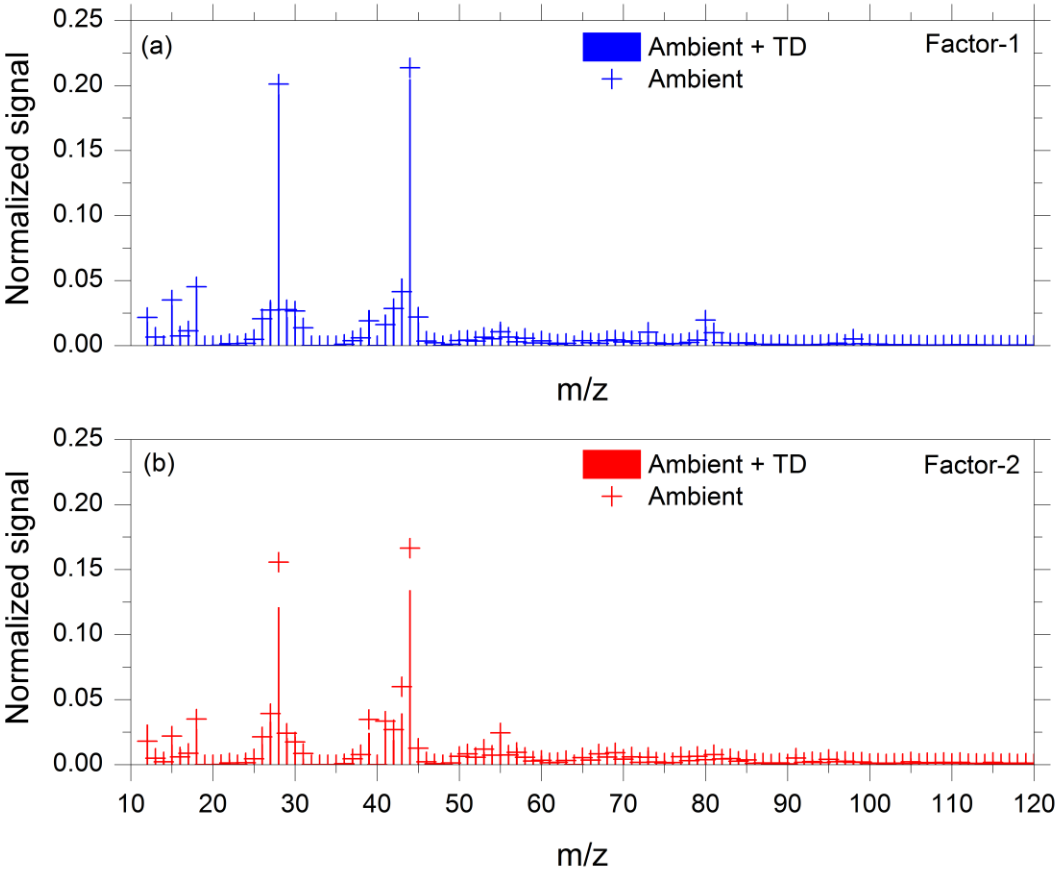

Figure S2: (a) Comparison of mass spectra of ambient OA PMF factor 1 analysis (crosses) and ambient plus thermodenuder PMF analysis (bars). (b) Comparison of mass spectra of ambient OA PMF factor 1 analysis (crosses) and ambient plus thermodenuder PMF analysis (bars).

Source apportionment of the OA was performed for the combined ambient and thermodenuded AMS spectra. This analysis was repeated by using only the ambient data, resulting in the same factors as for the complete dataset. Detailed analysis for the ambient organic components can be found in Florou et al. (in prep.). Kostenidou et al. (2009) proposed the theta angle (θ) as an indicator of mass spectra similarity by treating the AMS spectra as vectors and calculating their corresponding angle. Lower θ implies more similar spectra. Comparing the results of the PMF of only the ambient data and of the ambient plus TD spectra, the resulting angles were 4^o for Factor 1 and 8^o for Factor 2 suggesting that the ambient plus TD PMF analysis gave for all practical purposes the same factors as the ambient-only OA analysis. The ambient and TD mass spectra of the two factors are shown in Figure S2.

S2. Sensitivity analysis for the TD model

Sensitivity tests were performed in order to evaluate the behavior of the calculated volatility distributions to changes in the accommodation coefficient (a_m) and the effective vaporization enthalpy (ΔH_{vap}). First, the sensitivity of the volatility distributions to the accommodation coefficient were investigated using values ranging between 0.01 and 1. Both the volatility distribution and the effective vaporization enthalpy were recalculated, and the results were compared to the base case. The changes in the volatility distribution and the accommodation coefficient were also studied when the effective vaporization enthalpy ranged from 50 kJ mol^{-1} to 100 kJ mol^{-1}. The same sensitivity analysis was also performed for the volatility distributions of each PMF factor.

The measured and the predicted thermograms during the sensitivity tests to a_m are shown in Figure S3. When the a_m was reduced to 0.01, the mass transfer resistances during the OA evaporation increased. In this case we assume a slower OA evaporation compared to the rest of the cases with a_m=0.1, a_m=1 or a_m=0.27 (base case). The changes in the estimated volatility distributions were modest. A decrease of a_m resulted in general in a small increase of the estimated SVOC content. The estimated ΔH_{vap} values were 100, 88 ± 14, and 70 ± 19 kJ mol^{-1} for the cases of a_m =0.01, 0.1, and 1.0 respectively compared to the 80 ± 20 kJ mol^{-1} for the base case.

Figure S4 shows the predicted thermograms for ΔH_{vap} of 50 and 100 kJ mol^{-1}. For the reported base case, ΔH_{vap} was 80 ± 20 kJ mol^{-1}. The predicted thermograms for ΔH_{vap} of 50 and 100 kJ mol^{-1} reproduce the experimental observations relatively well, but with higher error than the base case model results. The differences for these cases are more pronounced for temperatures between 150 ^oC and 200 ^oC. Once again modest changes were found in the estimated volatility distributions when ΔH_{vap} varied from 50 kJ mol^{-1} to 100 kJ mol^{-1}. The ΔH_{vap} decrease to 50 kJ mol^{-1} resulted in a corresponding increase of SVOCs by almost 15%. The estimated a_m showed little variability compared to the base case value of 0.27.

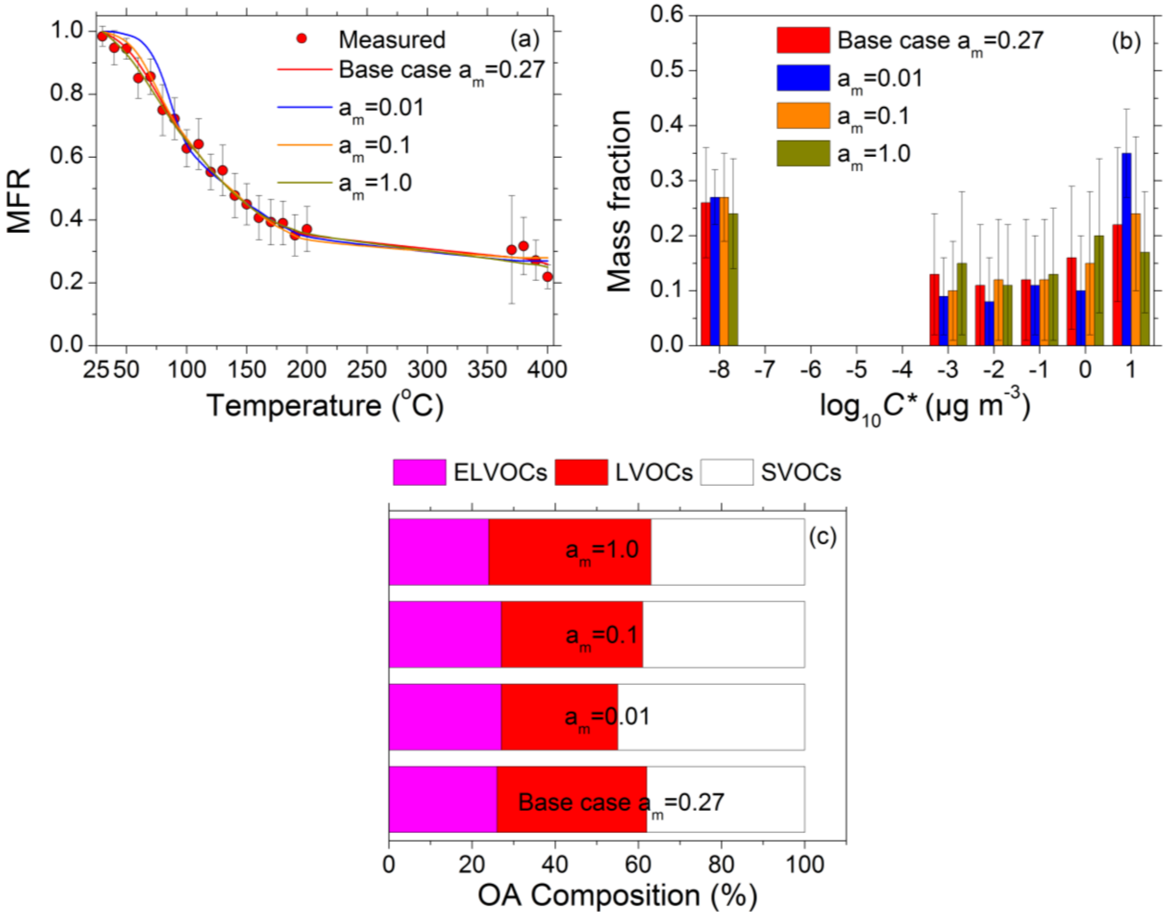

Figure S3: (a) Measured (red circles) and predicted thermograms for the base case (red line), a_m=0.01 (blue line), a_m=0.1 (orange line), and a_m=1.0 (dark yellow line) for total OA FAME-16 according to the model of Karnezi et al. (2014). The error bars represent ± 2 standard deviations of the mean. (b) Estimated OA volatility distributions for the base case and the sensitivity tests to different a_m values along with their corresponding uncertainties (± 1 standard deviation of the mean) according to the model of Karnezi et al. (2014). (c) OA composition for the different a_m values. ELVOCs are in magenta, LVOCs in red and SVOCs in white.

The changes in the volatility distributions for the two-factor solution obtained from the PMF analysis (MO-OOA and LO-OOA) are summarized in Figures S5 and S6. For the MO-OOA factor, when a_m was reduced to 0.01 mass transfer resistances during the evaporation increased resulting in slower evaporation of MO-OOA. The predicted thermograms were quite similar in all cases (Figure S5). The estimated vaporization enthalpy increased to 147 kJ mol^{-1} for a_m equal to 0.01 and 106 kJ mol^{-1} for a_m equal to 0.1 compared to the base case value of 89 kJ mol^{-1}.

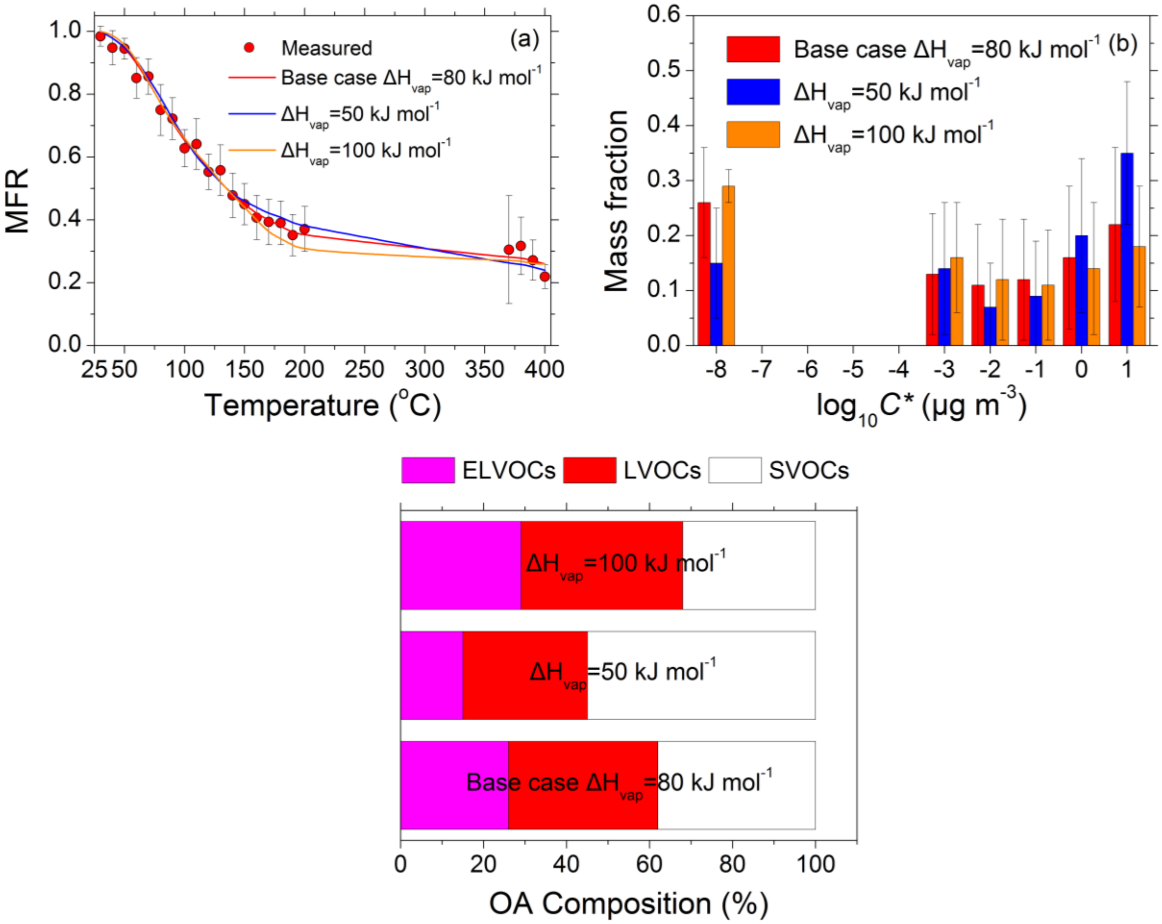

Figure S4: (a) Measured (red circles) and predicted thermograms for the base case (red line), ΔH_{vap} =50 kJ mol^{-1} (blue line) and ΔH_{vap} =100 kJ mol^{-1} (orange line) for total OA FAME-16 according to the model of Karnezi et al. (2014). The error bars represent ± 2 standard deviations of mean. (b) Estimated OA volatility distributions for the base case and the sensitivity tests to different ΔH_{vap} values along with their corresponding uncertainties (± 1 standard deviation of the mean) according to the model of Karnezi et al. (2014). (c) OA composition for the different ΔH_{vap} values. ELVOCs are in magenta, LVOCs in red and SVOCs in white.

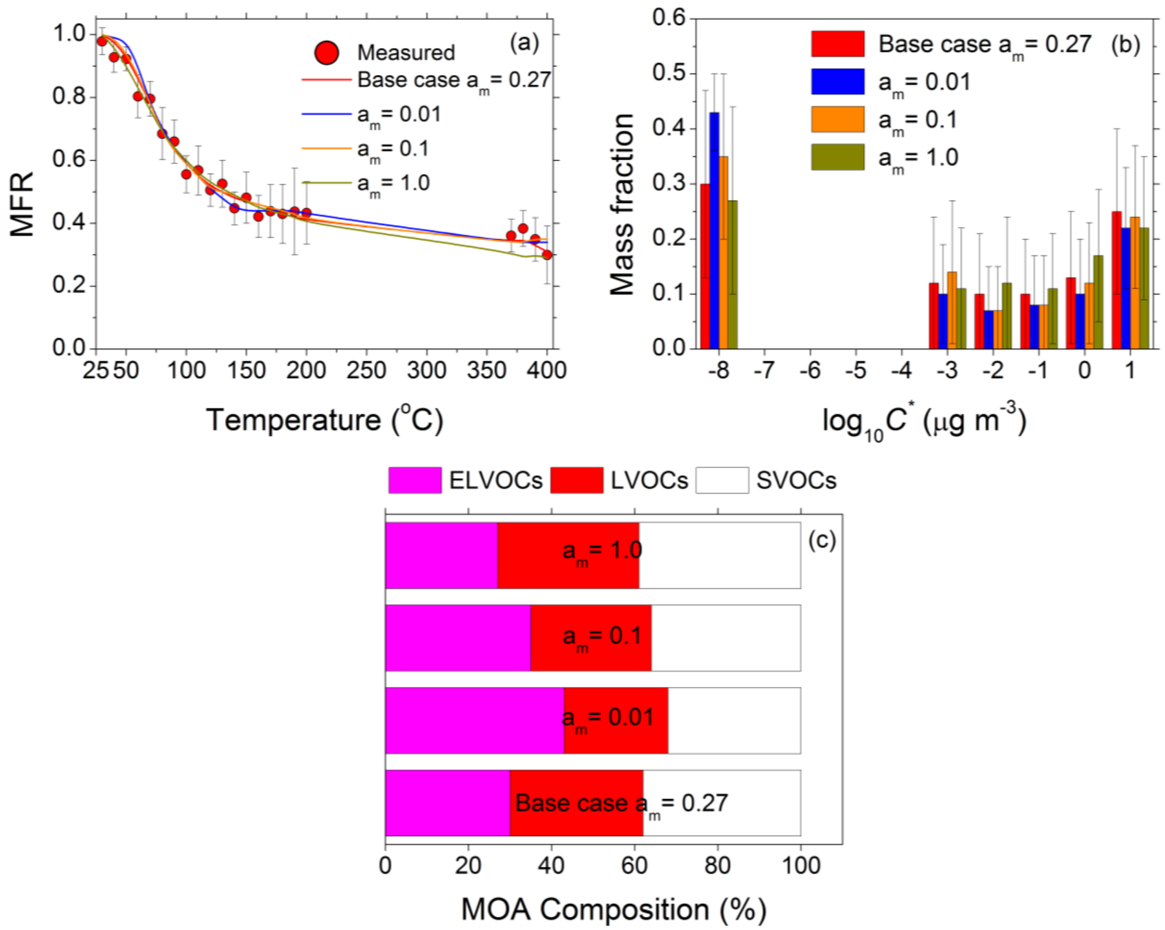

Figure S5: (a) Measured (red circles) and predicted thermograms for the base case (red line), a_m=0.01 (blue line), a_m=0.1 (orange line), and a_m=1.0 (dark yellow line) for MO-OOA FAME-16 according to the model of Karnezi et al. (2014). The error bars represent ± 2 standard deviations of the mean. (b) Estimated MO-OOA volatility distributions for the base case and the sensitivity tests to different a_m values along with their corresponding uncertainties (± 1 standard deviation of the mean) according to the model of Karnezi et al. (2014). (c) MO-OOA composition for the different a_m values. ELVOCs are in magenta, LVOCs in red and SVOCs in white.

Increasing the a_m to unity the vaporization enthalpy decreased to 71 kJ mol^{-1}. Its volatility distribution did not change significantly when a_m ranged from 0.01 to 1.0. The changes in the MO-OOA composition were modest for changing the a_m from 0.1 and 1.0 compared to the base case results. Only for the case of a_m equal to 0.01 the LVOC and ELVOC contents decreased and increased respectively by 10%. The same behavior was also obtained for the LO-OOA factor during the same test (Figure S6). The volatility distribution did not change significantly, when a_m was varied from 0.01 to unity. Its ΔH_{vap} increased also when a_m decreased to 0.01 compared to the base case value (67 kJ mol^{-1}). However, ΔH_{vap} remained almost constant for a_m equal to 0.1 and increased for a_m equal to unity. The LO-OOA composition remained similar during the a_m changes.

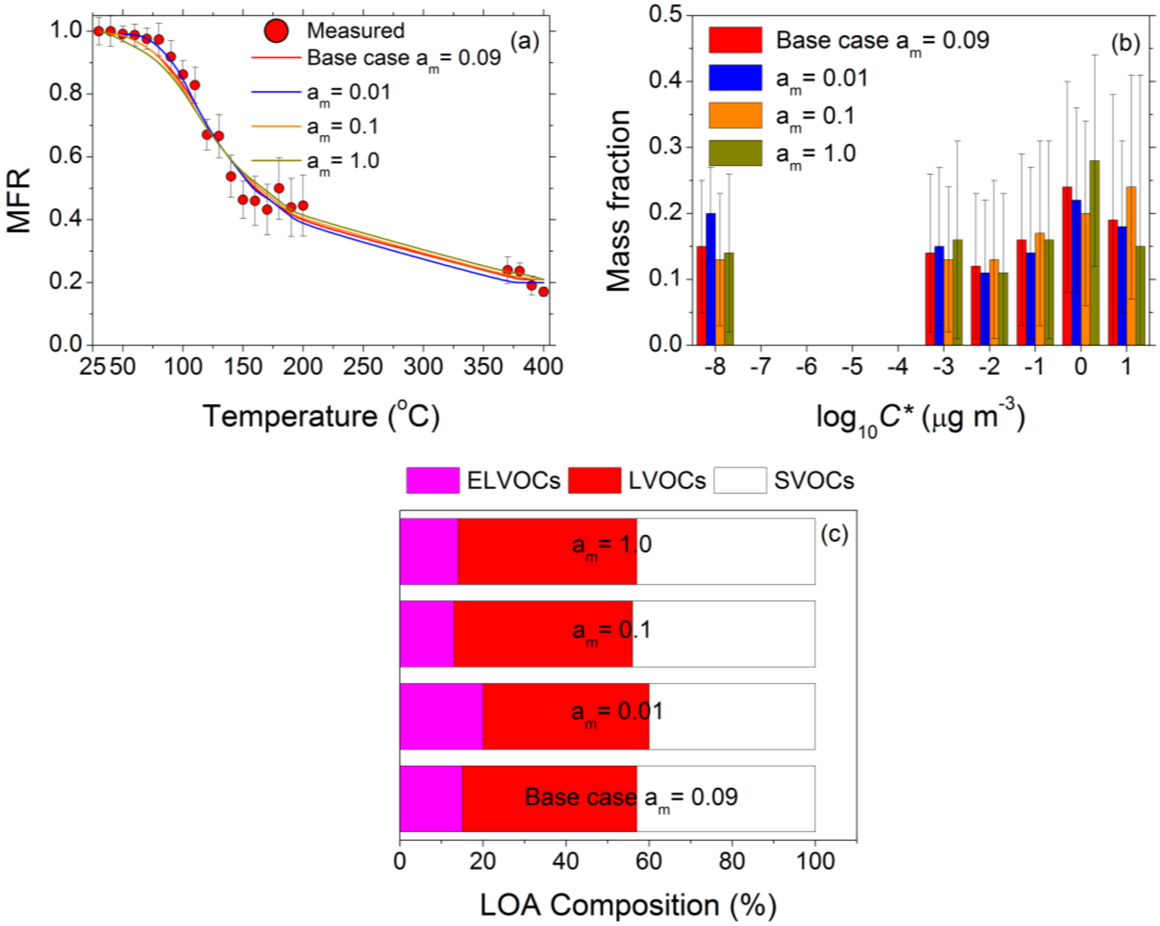

Figure S6: (a) Measured (red circles) and predicted thermograms for the base case (red line), a_m=0.01 (blue line), a_m=0.1 (orange line), and a_m=1.0 (dark yellow line) for LO-OOA FAME-16 according to the model of Karnezi et al. (2014). The error bars represent ± 2 standard deviations of the mean. (b) Estimated LO-OOA volatility distributions for the base case and the sensitivity tests to different a_m values along with their corresponding uncertainties (± 1 standard deviation of the mean) according to the model of Karnezi et al. (2014). (c) LO-OOA composition for the different a_m values. ELVOCs are in magenta, LVOCs in red and SVOCs in white.

References

Burtscher, H., Baltensperger, U., Bukowiecki, N., Cohn, P., Hüglin, C., Mohr, M., Matter, U., Nyeki, S., Schmatloch, V., Streit, N. and Weingartner, E.: Separation of volatile and non-volatile aerosol fractions by thermodesorption: Instrumental development and applications, J. Aerosol Sci., 32, 427–442, 2001.

Florou, K., Liangou, A., Louvaris, E., Kaltsonoudis, C., Tasoglou, A., Patoulias, D., Kouvarakis, G., Vlachou, A., Kourtchev, I. and Spyros N. Pandis, S. N.; The Finokalia Aerosol Measurement Experiment (FAME-16): Atmospheric processing of organic aerosol in the Eastern Mediterranean, in prep.

Hildebrandt, L., Engelhart, G. J., Mohr, C., Kostenidou, E., Lanz, V. A., Bougiatioti, A., DeCarlo, P. F., Prévôt, A. S. H., Baltensperger, U., Mihalopoulos, N., Donahue, N. M., and Pandis, S. N.: Aged organic aerosol in the eastern Mediterranean: The Finokalia aerosol measurement experiment 2008, Atmos. Chem. Phys., 10, 4167–4186, 2010.

Karnezi, E., Riipinen, I., and Pandis, S. N.: Measuring the atmospheric organic aerosol volatility distribution: a theoretical analysis, Atmos. Meas. Tech., 7, 2953–2965, doi:10.5194/amt7-2953-2014, 2014.

Kostenidou, E., Lee, B. H., Engelhart, G. J., Pierce, J. R. and Pandis, S. N.: Mass spectra deconvolution of low, medium, and high volatility biogenic secondary organic aerosol, Environ. Sci. Technol., 43, 4884–4889, 2009.

Kostenidou, E., Pathak, R. K., and Pandis, S. N.: An algorithm for the calculation of secondary organic aerosol density combining AMS and SMPS data, Aerosol Sci. Tech., 41, 1002–1010, 2007.

Louvaris, E.E., Florou, K., Karnezi, E., Papanastasiou, D.K., Gkatzelis, G.I., and Pandis, S.N.: Volatility of source apportioned wintertime organic aerosol in the city of Athens, Atmos. Environ., 158, 138-147, 2017.